COMMUNICATION

XXXX

ADVANCED
ENGINEERING
MATERIALS

www.aem-journal.com

Mechanical Properties of Graphene Foam and Graphene Foam—Tissue Composites

Katie M. Yocham, Crystal Scott, Kiyo Fujimoto, Raquel Brown, Emily Tanasse, Julia T. Oxford, Trevor J. Lujan, and David Estrada*

Graphene foam (GF), a 3-dimensional derivative of graphene, has received much attention recently for applications in tissue engineering due to its unique mechanical, electrical, and thermal properties. Although GF is an appealing material for cartilage tissue engineering, the mechanical properties of GF-tissue composites under dynamic compressive loads have not yet been reported. The objective of this study is to measure the elastic and viscoelastic properties of GF and GF-tissue composites under unconfined compression when quasi-static and dynamic loads are applied at strain magnitudes below 20%. The mechanical tests demonstrate a 46% increase in the elastic modulus and a 29% increase in the equilibrium modulus after 28-days of cell culture as compared to GF soaked in tissue culture medium for 24 h. There is no significant difference in the amount of stress relaxation, however, the phase shift demonstrates a significant increase between pure GF and GF that has been soaked in tissue culture medium for 24 h. Furthermore, the authors have shown that ATDC5 chondrocyte progenitor cells are viable on graphene foam and have identified the cellular contribution to the mechanical strength and viscoelastic properties of GF-tissue composites, with important implications for cartilage tissue engineering.

Prof. D. Estrada
Center for Advanced Energy Studies
Boise State University
1910 University Dr., Boise, ID 83725, USA
E-mail: daveestrada@boisestate.edu

K. M. Yocham, E. Tanasse, Prof. T. J. Lujan
Department of Mechanical and Biomedical Engineering
Boise State University
1910 University Dr., Boise, ID 83725, USA

Prof. D. Estrada, K. M. Yocham, K. Fujimoto
Micron School of Materials Science and Engineering
Boise State University
1910 University Dr., Boise, ID 83725, USA

C. Scott, R. Brown, Prof. J. T. Oxford
Biomolecular Research Center
Boise State University
Boise, ID 83725, USA

Prof. J. T. Oxford
Department of Biological Sciences
Boise State University
Boise, ID 83725, USA

1. Introduction

Hyaline cartilage, found at the surfaces of articulating joints, has a limited regeneration capacity, and as a result, cartilage injury can lead to osteoarthritis (OA). OA affects 21.6% of the U.S. population over the age of 18 and prevalence increases to 50% for those over the age of 65.[1] Worldwide, OA is the 11th leading cause of disability.[2] To date, prevention and cure for OA has eluded the scientific community and treatments are limited to symptomatic relief or total joint replacement. Current surgical treatment for OA includes arthroscopy to remove fragments of cartilage, arthroplasty for the resurfacing of the joint, and microfracture, a technique that attempts to regenerate articular cartilage by stimulating mesenchymal stem cells (MSC) located in the subchondral bone.[3–5] While MSCs can contribute to the successful formation of new cartilage, the new cartilage is often more fibrocartilage-like and the mechanical properties are insufficient to support the loads of the knee joint. This leaves the cartilage defect inadequately repaired, and can result in the need for additional surgeries.[3] Approaches such as matrix-assisted autologous chondrocyte implantation (m-ACI) involve the use of a hydrogel or polymer-based matrix such as collagen, hyauronan, or other polymers. Such matrices are seeded with autologous chondrocytes and glued into the defect site using fibrin glue.[6,7] However, m-ACI is limited by the rate of chondrocyte differentiation and growth and the potential for chondrocytes to undergo de-differentiation, marked by a change in collagen synthesis from type II to type I.[7] It has been shown that cells respond to the stiffness of their environment[8] therefore, in contrast to hydrogel or polymer-based matrices, a more mechanically robust scaffold material may be capable of facilitating articular cartilage tissue regeneration[9] by inspiring rapid stem cell growth and guiding stem cell differentiation toward the hyaline phenotype.

Graphene– a 2-dimensional crystal of hexagonally arranged carbon atoms– has captured the interest of multiple fields due to its unique mechanical, electrical, and thermal properties. Graphene has been utilized as a component of batteries,[10] within super capacitors,[11] for its electrochemical sensing capabilities,[12,13] and more recently in the field of tissue

engineering.[9,14–17] Specifically, the three dimensional analog of graphene, graphene foam, (GF) has recently been shown as an effective bioscaffold for stem cell growth and differentiation along various neuronal and musculoskeletal lineages.[14–17] These GF-tissue composites are not only biocompatible, but they also promote rapid cell attachment,[18] proliferation, and the spontaneous osteogenic differentiation of human mesenchymal stem cells (hMSCs).[15] GF creates a biomimetic microenvironment that allows for good nutrient and waste transport[18] and its high specific surface area facilitates good cell attachment.[15] GF also affords the unique capability to provide highly conductive pathways for electro-active cells or electrical stimulus for those cells which experience directed differentiation under such stimulation.[17,19] Importantly, the term "graphene foam" has been used in the literature to define various types of 3D carbon based foams which are not composed entirely of atomically thin 2D graphene. This nomenclature has been adopted to describe foams composed of stacked exfoliated graphene flakes as well as ultrathin graphitic foams grown by chemical vapor deposition (CVD) with regions of single layer graphene. Li et al. have demonstrated the enhanced growth of neural stem cells under electrical stimulation on GF,[18] and recently, we have shown that muscle cells on a GF scaffold respond to electrical stimulus.[14] It is well known that charge plays a critical role in maintaining the osmotic pressure of articular cartilage,[20] and electrical stimulation has been shown to significantly increase cell proliferation, glycosaminoglycan (GAG) synthesis, and the upregulation of extracellular matrix genes in 3D and 2D models of cartilage.[21]

Recent studies have shown that cells respond to the stiffness of the underlying substrate.[22,23] 2D graphene has one of the highest elastic moduli of any other material (≈1 TPa) and GF's unique structure, composed of hollow branches and node junctions that are formed as numerous 2D graphene layers are deposited on top of one another by CVD, provides the cell both high stiffness of the

graphene and/or graphite surface at the cellular level, as well as abundant anchor points due to the 3D structure and wrinkles in the GF surface. GF also affords the ability to modify the physical characteristics such as pore size, which can affect the ability to meet metabolic demands by controlling the mass flow of nutrients and waste, or density to achieve tissue-specific scaffold mechanical properties.[24] GF's surface chemistry can be altered using various biopolymers to tune its strength and surface energy characteristics to meet the requirements of different cell lines.[17,25,26] The electrical properties of GF allow for electro-mechanical stimulation and it has been shown that the conductivity of GF remains stable with no production of harsh byproducts, unlike conductive polymers.[27] Finally, graphene materials demonstrate antibacterial and antifungal properties in wound infection, suggesting potential for anti-infective properties in tissue engineering applications.[28,29]

The impressive stiffness of 2D graphene is not evident in quasi-static mechanical measurements of bulk 3D GF. Several methods have been utilized in order to measure the quasi-static, or elastic, stiffness of GF. Nieto et al. used nanoindentation and the volume-based Gibson-Ashby relationship to estimate the strength of bulk CVD GF.[30] In a subsequent publication, Nieto et al. used similar methods to evaluate a polymer-strengthened GF matrix and demonstrated GF as a suitable scaffold for hMSCs, however, the mechanical properties of the GF-tissue composites were not reported.[17] Park et al. studied CVD GF in bulk unconfined compression and demonstrated a power-law dependence of compressive mechanical properties to GF density.[24] There have been other studies performed on GFs prepared using graphene oxide that are summarized in **Table 1**. In a previous study using CVD GF as a substrate for cartilage tissue regeneration,[17] the mechanical testing procedures did not include the testing of GF-tissue composites in unconfined compression, a standard method to characterize cartilage

Table 1. Mechanical properties of graphene-based bioscaffolds.

Synthesis method	Bioscaffold	Pore size/Density [mg cm^{-3}]	Mechanical property	Cell line	Ref.
CVD	GF	580 μm/4	Comp. modulus: 12.7 ± kPa Stress relaxation: 9.9 ± 3.4% Dynamic modulus: 27 ± 3.4 kPa Phase shift: 0.11 ± 0.013 rad	ATDC5	Present study
	GF	580 μm/4	—	C2C12	[14]
	GF/PDMS	≈400 μm before PDMS/ ≈5	Tensile modulus ≈18 Mpa	Not tested	[39]
	GF/PVDF GF/PCL	—/—	—	Tested bio-mineralization only	[38]
	GF/PLC	100–200 μm/0.005	Tensile modulus 254.0 ± 43.7 kPa	hMSCs	[17]
	GF	100—300 μm/—	—	NSCs	[18]
	GF	>100 μm/ ≈320 g m^{-2}	—	hMSCs	[15]
	GF/Hydroxy-apatite	100–300 μm/—	Comp. modulus 0.9 MPa	MC3T3-E1 Osteoblasts	[25]
	GF/PLGA/CTS	≈310 μm/—	Tensile strength: 47–150 kPa	hMSCs	[26]
GO	CSMA/PECA/GO	152.8–193.5 μm/—	Unconfined compressive modulus 0.48 MPa	3T3s and cells harvested from rabbit cartilage	[9]
	Chitosan/PVA/GO	—/—	Tensile modulus: 1.81, 2.78 MPa for 0.4 wt% and 0.6 wt% GO concentration, resp.	ATDC5	[51]

**ADVANCED
SCIENCE NEWS**

www.advancedsciencenews.com

**ADVANCED
ENGINEERING
MATERIALS**

www.aem-journal.com

tissue.[20,30–32] While GF shows promise in the field of cartilage tissue engineering, the compressive mechanical properties of GF-tissue composites have not been reported.

In addition to the study of the quasi-static mechanical properties of GF, several studies have demonstrated that GF does exhibit a time-dependent mechanical response. Nautiyal et al. studied the damping behavior of GF and proposes three multiscale dampening mechanisms of GF: rippling in individual graphene sheets, van der Waals forces dominating the interactions between individual graphene layers, and branch bending at the structural level.[33] The 3D interconnected node-branch anatomy of GF is advantageous to ripple wave propagation, and thus energy dissipation,[33–35] and molecular dynamic simulations of ripples in graphene demonstrate how a ripple wave might split when the wave encounters a physical defect, thus assisting in the dissipation of impact force.[36] These previous studies have advanced our understanding of damping mechanisms in GF, but the damping mechanisms of GF-tissue composites in unconfined dynamic compression is currently unknown. No study has reported the time-dependent viscoelastic properties of GF-tissue composites, which are critical outcome measures for cartilage replacement tissue as they represent energy dissipation from interstitial fluid flow and deformation of the solid matrix.[37]

Therefore, this study seeks to perform non-destructive mechanical testing of GF and GF-tissue composites in unconfined compression to determine a baseline measurement of the elastic and viscoelastic compressive mechanical properties of GF and the relative change in these properties due to the addition of cells.[17,26,38] Additionally, we aimed to elucidate time dependent changes in the mechanical properties of GF scaffold as chondroprogenitor cells (ATDC5) are cultured over a period of 28 days.

2. Results and Discussion

2.1. Graphene Foam Synthesis and Characterization

The GF used in this study (Graphene Laboratories Inc., Calverton, NY, USA) was grown using CVD,[39] whereby decomposed methane and hydrogen gasses flow past the nickel (Ni) foam templating agent at 1000 °C causing carbon to precipitate on the surface of the Ni foam. The resulting Ni/GF substrates are then etched in iron tricholoride ($FeCl_3$) to remove the Ni substrate, resulting in a freestanding GF with a typical pore size of 580 μm. To understand the microstructure of our scaffolds, the GF was imaged by scanning electron microscopy (SEM) (FEI Teneo, Waltham, MA). SEM images show the macroporous structure, with higher magnifications highlighting wrinkling in the graphene due to the difference in thermal expansion coefficients between the underlying Ni substrate and the overlaid graphene (**Figure 1**a–c).[39] While studies have demonstrated the ability of single layer graphene to enhance serum protein adsorption, and thus cell adhesion,[15,40] the addition of wrinkles GF are likely an advantage to anchorage-dependent cells, as surface roughness further enhances cell adhesion to GF, which is essential for cell proliferation and function.[18]

To determine the quality of the GF, we used Raman spectroscopy (HORIBA Instruments Inc., Edison, NJ). Figure 1d and e show Raman maps of the characteristic G ($\approx 1580\ cm^{-1}$) and 2D peak ($\approx 2700\ cm^{-1}$) intensities for our GF samples (I_G and I_{2D}, respectively). These maps consist of 100 point spectra over a 36 μm by 36 μm, collected on a 4 μm step. Figure 1f shows the I_{2D}/I_G ratio, highlighting the predominately
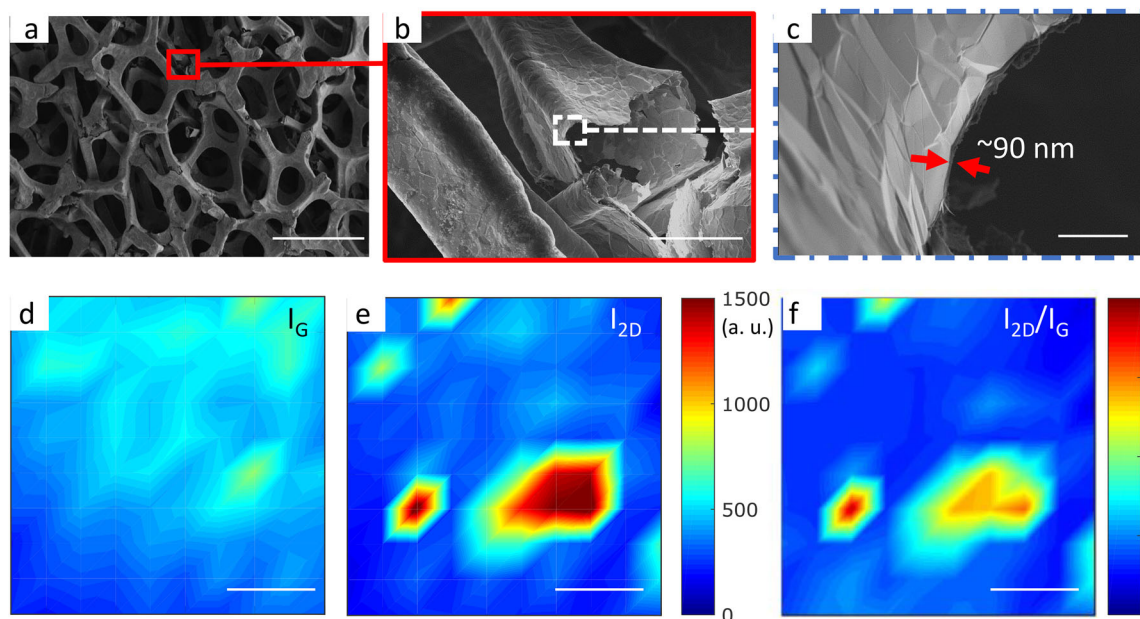
Figure 1. SEM and Raman characterization of CVD graphene foam. SEM images of GF show the a) branched structure with pore sizes ≈200–500 μm in diameter, b) a magnified image of a broken branch interconnect, and c) approximate sidewall thickness. Scale bars in a–c) are 500, 50, and 2 μm, respectively. Raman maps of d) G-peak intensity (I_G at ≈1580 cm^{-1}) e) 2D peak intensity (I_{2D} at ≈2700 cm^{-1}), and the f) I_{2D}/I_G ratio. Raman intensity mapping demonstrates the predominately graphitic nature of CVD GF, with few monolayer regions where $I_{2D}/I_G > 2$. Scale bars in d–f) are 10 μm.

ultrathin graphitic nature of our GF samples, with 94% of the spectra having an $I_{2D}/I_G < 2$, consistent with previous reports using the GF nomenclature.[15–18,39] The absence and/or low intensity of the characteristic D peak ($\approx 1350\,cm^{-1}$) indicates the GF has a low defect density (see Supporting Information Figure S1). Hence, CVD GF is likely to exhibit excellent charge carrier mobility, due to low defect density and a lack of inter-sheet junction contact resistance, as compared to graphene foam synthesis by freeze drying or template assembly methods.[18,39]

To provide a quantitative measure of porosity and density, the GF was imaged and analyzed via X-ray diffraction and with a SkyScan 1172 Xray MicroCT (Bruker MicroCT, Kontich, Belgium) (see Supporting Information Figure S2). The GF was calculated to have a surface area to volume ratio of $144.16\,mm^{-1}$, an object volume to total volume ratio (Obj.V/TV) of 13.30% corresponding to a porosity of 86.70%, and an average structure thickness (St.Th) of $22.93 \pm 6.0\,\mu m$. Similar to gelatin scaffolds, the porosity of the GF may allow for good nutrient transport and waste removal.[9] The large GF pore size also allows chondrocytes to maintain their typical phenotype as previous studies have shown increased proliferation and extracellular matrix production when the scaffold pore sizes range between 250 and $500\,\mu m$.[41] Following physical characterization of our GF samples, mechanical characterization of the GF scaffolds was performed on bare GF scaffolds, while ATDC5 cells were cultured on GF in preparation for mechanical testing of GF-tissue composites.

2.2. Cell Culture

The ATDC5 cell line is a chondroprogenitor cell line derived from mouse teratocarcinoma cells and is well-established as an in vitro model to observe cell signaling pathways during chondrogenesis.[42] GF was seeded with ATDC5 chondroprogenitor cells, cultured initially for 24 h in growth medium (GM), at which point the tissue culture medium was exchanged with differentiation medium (DM). Cell growth on GF was monitored with a light microscopy; bright-field transmitted light images were acquired throughout the cell culture period. Representative images from cell culture at 24 h, and 7, 14, 21, 28 days after cell seeding can be seen in **Figure 2**a–d. ATDC5 cells adhered to the GF during within 24 h of cell culture, (Figure 2a); are seen spanning the pores of the GF by 7 days, (Figure 2b); and filling the pores of the GF by 14 days of culture (Figure 2c,d). While transmitted light images emphasize the ability of ATDC5 cells to adhere and proliferate on GF, immunofluorescent labeling and confocal microscopy were used to demonstrate successful cell proliferation throughout the 3D bioscaffold (Figure 2e–p; Supporting Information Movie S1).
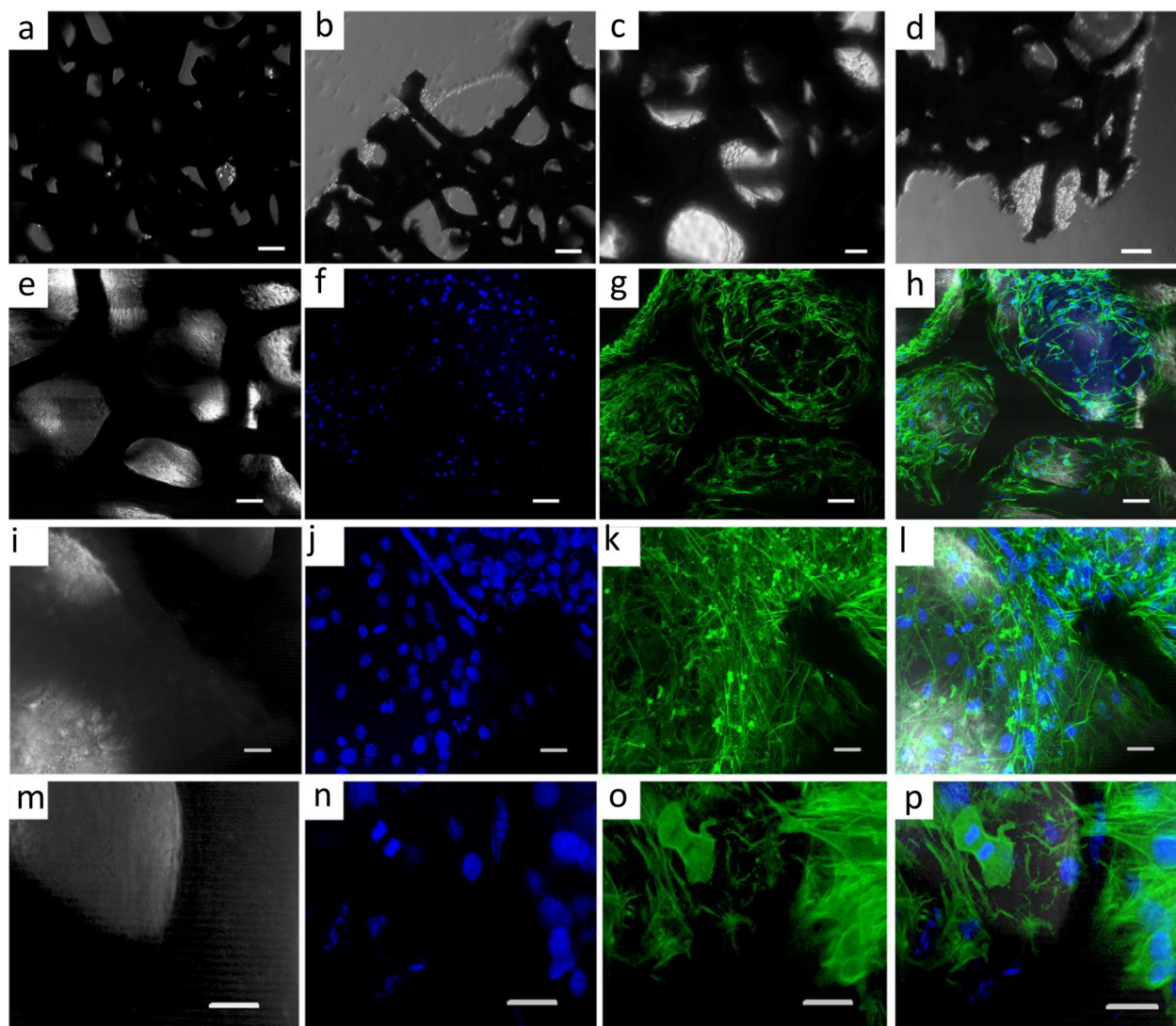
2.3. Mechanical Testing

To understand the biomechanical relevance of GF scaffolds for cartilage engineering, we developed a testing protocol to measure the elastic and viscoelastic properties of GF in unconfined compression (**Figure 3**a–c). Unconfined compression closely resembles the conditions found in the cartilage near the articulating surface, with the potential for high fluid flow and low hydrostatic pressure.[37,40,43] To elucidate the changes in the load dissipation mechanisms during cell growth and differentiation; these properties were measured both with and without chondroprogenitor cells grown on the scaffold.

Several studies[44–46] demonstrate a rubber-like constitutive response of GF with three distinct regions: elastic, plateau, and densification. The first is due to elastic branch bending. Once compression has exceeded the elastic region, branch breaking occurs and results in a plateau in the stress strain curve. Finally, a sharp increase in stress indicates the region in which the branches begin to compact; this is the densification region. To first determine the elastic region of the GF, a quasi-static mechanical test was performed to 40–50% strain (Figure 3b). The elastic regime of the GF used in this study was determined to lie within 0–20% strain ($n = 3$). In this study, all subsequent samples were tested using a maximum compressive engineering strain of 14% in order to remain well below the plateau region where plastic deformation of the GF occurs. Interestingly, this study had a less visible plateau region than prior studies. A study by Park et al., where GF of density $4\,mg\,cm^{-3}$ was tested up to 100% strain, showed an elastic region between 0% and 10% strain, a plateau region between 10% and $\approx 65\%$ strain, and a densification region between $\approx 65\%$ strain and 100% strain.[24] The discrepancy between the elastic region measured by Park et al. and in this study may be due to a much smaller preload used in the Park study, although the preload force was not reported by Park et al. Furthermore, the Young's modulus determined by Park et al. ($\approx 16\,kPa$) agrees well with the Young's modulus determined in this study ($\approx 13\,kPa$).

The dynamic testing protocol (Figure 3c) contained specific steps to measure the compressive linear modulus, equilibrium modulus, dynamic modulus, phase shift, and stress relaxation of the samples. The compressive linear modulus and equilibrium modulus provide measures of the elastic properties of the GF and GF-tissue composite; the dynamic modulus, phase shift, and stress relaxation provide a measure of the material's viscoelastic properties, which are critical for normal cartilage function. Results from our mechanical testing protocol are summarized in **Figure 4**. The mechanical tests demonstrate a $\approx 46\%$ increase in the elastic modulus, a $\approx 29\%$ increase in the equilibrium modulus, and a $\approx 30\%$ increase in dynamic modulus after 28-days of cell culture as compared to the conditioned GF (GF soaked in tissue culture medium for 24 h). (Figure 4a,b), These increases in modulus can be interpreted relative to a prior study by Nieto et al., who used in situ SEM to observe the deformation mechanisms of GF using nanoindentation. Nieto et al. identified branch bending and indentation as the primary mechanism by which foams break in compression,[30] noting that the strength of the GF is highly impacted by the number of defects found in the foam.[33] In a subsequent study, Nieto et al. demonstrated a significant increase in GF strength with the addition of a polymer; suggesting that strengthening of the GF-polymer matrix is due to the filling of voids and defects in the GF.[17] Likewise, as ECM molecules are produced by the ATDC5 cells, it is possible that these load-bearing molecules may also contribute to the GF strength by the filling of voids and defects, as atomistic studies predict bulk modulus values of 8 GPa for collagen and up

ADVANCED
SCIENCE NEWS
www.advancedsciencenews.com
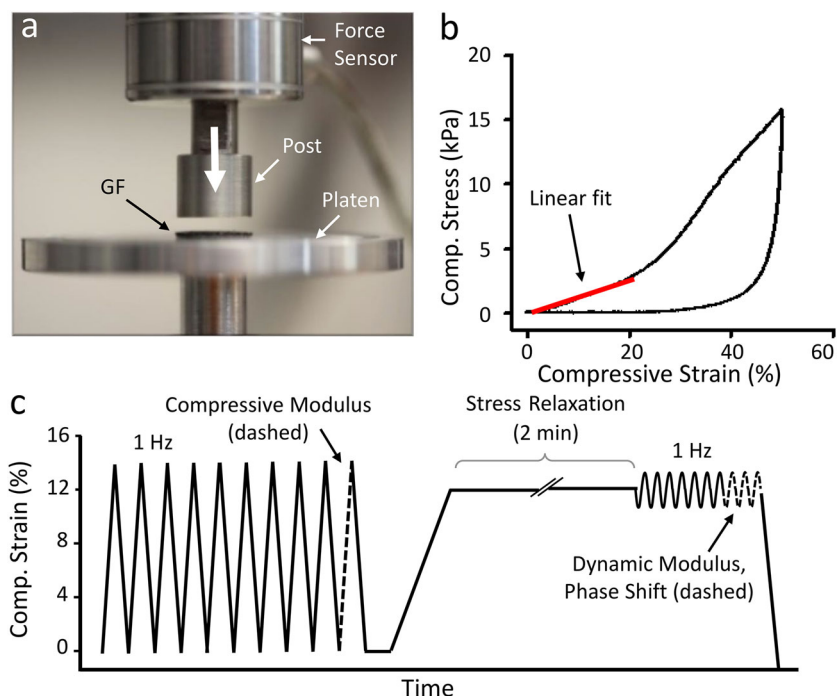
ADVANCED
ENGINEERING
MATERIALS
www.aem-journal.com

Figure 2. ATDC5 cells grown on graphene foam: a–d) Transmitted light images depict the cell growth after a) 24 h, b) 7 days, c) 14 days, and d) 21 days. e–p) Confocal Microscope image after 28 days cell growth. Panel e–h) 20× immunofluorescent image −single plane. Panel i–l) 40× maximum image projection of a 50 μm Z-stack. Panel m–p) 40× maximum image projection of a second 50 μm Z-stack. e), i), m) transmitted light; f), j), n) DAPI stain nucleus; g), k), o) AF488-phalloidin stain for actin; h), l), p) merged image transmitted light, DAPI, Actin. Scale bar in a) and b) 100 μm; c–h) 50 μm; i–p) 20 μm.

to 35 GPa for collagen under a 5 GPa hydrostatic pressure.[47] This may explain the increase in modulus values we observed after culture.

No significant change was observed with respect to the measure of stress relaxation. (Figure 4c) The ≈22% increase in stress relaxation between conditioned GF and GF at day 14 of cell culture may due to an increased proteoglycan production, but would need to be verified by biochemical analysis. The phase shift for a wetted GF scaffold (0.11 ± 0.014 rad) was 53% of the reported phase shift for articular cartilage (15°, or 0.26 rad[31]). It is interesting to note that materials primarily comprised of collagen have a phase shift of 3.4°,[37] proteoglycan-rich materials have a phase shift angle of ≈70 degrees,[48] while articular cartilage, composed of both proteoglycans and collagen in varying amounts, has been shown to have a phase shift of

≈15°.[31] This suggests that GF, before culture with cells or media, displays a phase shift between primarily collagenous materials and articular cartilage. Furthermore, we observed that the measured phase shift seemed to be independent of cell culture, showing a significant increase for conditioned GF only (0.17 ± 0.004 rad) as compared to pure GF. This may be due to protein adsorption, as Lee et al. found that within 24 h graphene films and graphene oxide adsorbed up to 8% and 25%, respectively, of serum proteins in the tissue culture media.[40] Altering the surface properties of GF by protein adsorption may potentially increase the ability for dynamic load dissipation by the ripple propagation mechanism suggested by Nautiyal.[35] We believe the subsequent decrease in phase shift may be due to the production of ECM proteins, providing additional elasticity to the GF-tissue composite, as seen in the increasing trend in both

ADVANCED
SCIENCE NEWS

www.advancedsciencenews.com

ADVANCED
ENGINEERING
**MATERIALS**

www.aem-journal.com

Figure 3. Mechanical characterization protocol of GF and GF-tissue composites. a) The testing apparatus was assembled to compress the GF with homemade compression platens. b) A typical stress–strain curve for GF displays elastic behavior between 0% and 14% compressive strain. c) The testing method designed to measure the quasi-static and viscoelastic compressive properties of GF with and without cell culture (not drawn to scale).

the elastic modulus, equilibrium modulus, and dynamic modulus.

As commonly observed in cartilage tissue in compression,[48] the dynamic modulus at 28 days of cell culture was 33% greater than the equilibrium modulus at 28 days of cell culture because the interstitial fluid pressure of cartilage is maintained under cyclic loading but not under equilibrium conditions. Although we expected an increase in the viscoelastic properties, stress relaxation and phase shift, over the duration of cell culture, there was no evident trend. However, we do find consistency in the ratio of dynamic modulus to equilibrium modulus among groups (Figure 4b,d). This would suggest that the time-dependent mechanisms of GF in compression remain unaffected by cell culture; instead, cell culture primarily contributes to the elastic strength of the GF-tissue composite by the production of load-bearing ECM proteins. Furthermore, observed increases in phase shift after 24 h in a viscous media (Figure 4d) appear to be counteracted over time by the production of ECM proteins.

Although the equilibrium modulus of our GF-tissue composite composed of murine ATDC5 cells was yet an order of magnitude lower than reported for the equilibrium
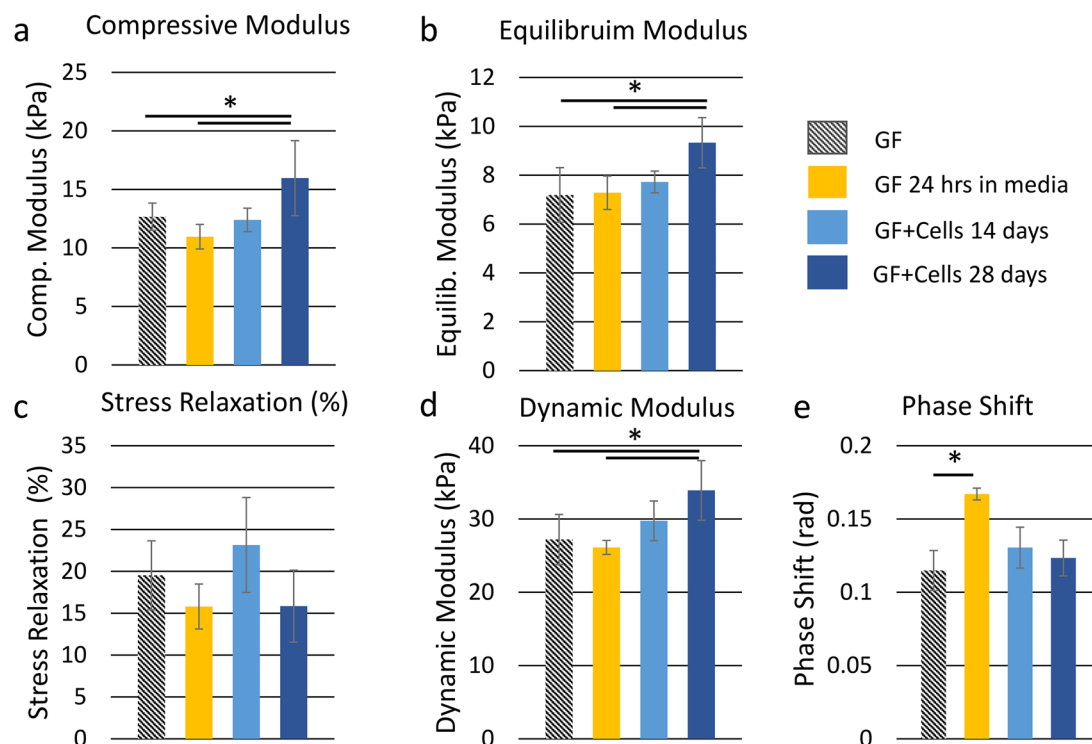
Figure 4. The measured quasi-static a), b) and viscoelastic c–e) properties of conditioned graphene foam (GF), graphene foam after 14 days of cell culture in chondrogenic medium (GF + C 14 days) and graphene foam after 28 days of cell culture in chondrogenic medium (GF + C 28 days).

modulus of adult human cartilage tissue measured using unconfined compression (0.24–0.85 MPa),[31] it was comparable to m-ACI solutions ($\approx$50 kPa)[49,50] and still shows promise in the area of guiding and improving cell differentiation as demonstrated in the current study by the increase in the compressive and equilibrium modulus of the GF-tissue composite with time in culture.

In order to place our results in perspective, we compare the mechanical performance of our GF-tissue composites to recent results in the literature. Table 1 provides an overview of bioscaffolds that are either graphene-based or utilize graphene as a strengthening mechanism. This table highlights the variation in mechanical properties due to testing mechanism, graphene synthesis methods, and the addition of natural and synthetic polymers. CVD GF has been shown to support the growth of ATDC5 chondroprogenitor cells, C2C12 mouse myoblast cells,[14] MC3T3-E1 osteoblasts,[25] hMSCs,[15–17,26] and neural stem cells.[18] The mechanical properties of CVD GF are dependent on both the template structure and the density of graphene deposited on the template.[24] Graphene oxide (GO) has been shown to support the growth of the 3T3 rabbit cartilage cell[9] line as well as ATDC5 chondroprogenitor cells.[51] GO has been used specifically to add mechanical robustness to porous hydrogels used for cartilage tissue engineering. While GO is effective as a mechanical strengthening mechanism in hydrogels, GO does not exhibit high electrical conductivity as it is an electrical insulator.[52] Although not performed in the current study, GF scaffolds can be utilized to facilitate the electrical stimulation of cells during the culture period to potentially enhance ECM production, and thus, engineer the mechanical properties of the tissue composite. As can be seen from the variation of methods, in Table 1, the mechanical study of the compressive properties of ATDC5 cells within a GF scaffold presented here serves to establish a baseline and standardized protocol for future studies aimed at identifying the mechanical performance of engineered GF-cartilage tissue composites.

3. Conclusion

This study demonstrates the viability of ATDC5 cells over 28 days on GF. GF grown by CVD provides a favorable microenvironment with both adequate porosity for nutrient transfer and waste removal as well as wrinkles and discontinuities for good cell attachment. Micro-CT was used to determine the porosity and density of the foam and SEM was used to gain insight into the structure of the GF. Transmitted light images were taken at specific time points to monitor cell adhesion, growth, and proliferation within the GF scaffold. Images of immunofluorescent phalloidin staining for actin revealed cell viability and good adhesion to the GF scaffold. As GF and GF-based scaffolds continue to be utilized for musculoskeletal tissue engineering, this study provides a baseline measurement of both the quasi-static and viscoelastic mechanical properties of GF in unconfined compression. Unconfined compression was used to reflect the conditions of the upper zones of cartilage with high fluid flow. Stress relaxation, dynamic modulus, and phase shift was measured to evaluate the viscoelastic properties of GF-tissue constructs in compression before and after cell culture with

ATDC5s. Additionally, we detect differences in mechanical properties between pure GF and GF which has supported cell growth and differentiation for 14 and 28 days. Although the increase in viscoelasticity, as shown by the phase shift and stress relaxation measurements, were not statistically significant over the cell culture period, we did demonstrate the ability of the testing method to detect statistically significant increases in other mechanical properties such as the compressive, equilibrium, and dynamic moduli. As suggested by prior studies[37] this strengthening of the elastic properties of the GF tissue composite may suggest a collagen-rich composite, which is vital for the regeneration of cartilage tissue.

Experimental Section

1 GF: The GF was analyzed with Raman spectroscopy (HORIBA Instruments Inc., Edison, NJ) to determine the average number of layers of the foam and to verify the complete removal of Ni. Raman spectroscopy was performed with a 532 nm excitation wavelength over a 36 μm by 36 μm area on a 4 μm step, resulting in 100 spectra. The GF was then imaged via scanning electron microscopy (SEM) (Hitachi S- 3400N − II, Tokyo, Japan) and X-ray diffraction (XRD) (Rigaku Miniflex 600). The GF was also imaged and analyzed with a SkyScan 1172 X-ray MicroCT (Bruker, Kontich, Belgium). Briefly, GF samples were transferred from solution, mounted onto a small filter and allowed to dry fully overnight. The GF/filter was placed upright on the z-axis of the sample holder, centered and secured to eliminate scan artifacts due to random movement. Scan data was acquired with an X-ray tube setting of 34 kV, 210 μA, and an exposure time of 325 ms; scan parameters for the 180° scan were defined with a step size of 0.1 degrees, 15-frame averaging and a pixel size of 6.06 μm. Cross section images were reconstructed from the shadow projections utilizing NRecon software (version 1.6.10.4) based on the Feldkamp algorithm. Skyscan CT Analyzer (CTan) software (version 1.15.4.0) was utilized to perform quantitative analysis and generate 3D models: GF object volume, structure thickness and surface area were calculated based on 3D models generated using the Adaptive rendering algorithm after binarization of the reconstructed slices.

2 Mechanical Testing: Mechanical tests were performed using the Instron 10 000 ElectroPuls system (Instron, Norwood, MA) and a custom stainless steel compression platen which was 8 mm in diameter (Figure 3a). Specimens (10 × 10 × 0.5 mm thickness) of bare GF ($n = 10$), conditioned GF ($n = 3$), and graphene which had undergone 14 days ($n = 5$) and 28 days ($n = 10$) of unconstrained cell culture with ATDC5 cells and chondrogenic differentiation medium were tested in unconfined compression. Five samples were used to determine the mechanical properties at day 14 of culture due to material constraints; it was desired to conduct all mechanical testing on the same batch of GF because of mechanical property variation between batches. The square dimensions of the specimens were cut using a razor. The 8 mm diameter of the upper testing platen was slightly smaller than the square dimensions of the GF specimens, and therefore any damaged graphene at the cutting surface should not affect the properties of the foam being characterized. The specimen thickness was left as received from the manufacturer, and no further leveling of the specimens was performed. For all sample sets, the GF was taken directly out of it's respective media and tested immediately; the samples were saturated with, but not submerged in media during mechanical testing.

In order to first determine the elastic region of the GF, the bare GF was preloaded to 0.02, which was a nominal preload within the measurement range of the 10 N load cell. This preload step provided uniform platen contact with the entire GF surface prior to testing, and therefore ensured a level testing surface. The preload was followed by a preconditioning protocol of ten sinusoidal waves to 10% strain at 0.5 Hz and subsequent quasi-static compression to 40–50% at 0.01 mm s^{-1} strain rate. A slower strain rate was appropriate for this test as we were interested in the quasi-static mechanical

properties of the GF. Using a custom MATLAB code, the resulting stress–strain curves were linearly fit between 5% strain and 20% strain where the R^2 values were >0.99 ($N = 3$) (Figure 3b). Subsequent testing was performed to a maximum of 14% in order to remain well within the elastic region of the foam.

The mechanical properties of the specimens were measured using a multi-step testing method in displacement control. Figure 3c depicts the testing method, consisting of a preload to 0.02 N, cyclic preconditioning to 14% compression at 0.5 Hz (Figure S3), ramp loading to 12% compression, 2 min of relaxation, and then dynamic loading via cyclic compression at 1% amplitude. The ramp loading was performed at 0.1 mm s^{-1}; this loading rate allowed the measurement of time-dependent stress relaxation while minimizing error that occurs at faster loading rates due to instrument overshoot of the targeted ramp displacement. The dynamic loading was carried out at 0.5 Hz as it is a physiologically relevant frequency for articular cartilage due to activities such as walking. Stress-strain curves were computed using the ratio of stress (F/a_o where F is the instantaneous force and a_o is the constant platen diameter) and engineering strain (($h–h_o)/h_o$ where h is the instantaneous sample thickness and h_o is the original sample thickness after 0.02 N preload). The compressive modulus was measured in the final compression of the precondition step. The compressive portion of the stress and strain data was linearly fit with $R^2 > 0.97$. The percent of stress relaxation was measured by comparing the peak stress reached after compression to 12% strain to the stress at the end of a 2 min stress relaxation period. Due to instrument limitations, the peak strain was up to 3% higher than the strain set point. It was determined, due to the logarithmic nature of the stress relaxation measurement, to be more accurate to begin measurements from the peak strain rather than beginning measurements once the instrument had equilibrated at 12% strain. The equilibrium modulus was calculated as the ratio of stress to strain at the end of the stress relaxation period. The dynamic modulus was calculated by fitting the last three sinusoidal compression cycles of the stress-time and strain-time data to a four parameter sine wave function ($R^2 > 0.96$ for all experiments) and dividing the amplitude of stress by the amplitude of strain. The phase shift was determined by subtracting the fitted phase parameters from the stress-time and strain-time data.[53] The effect of culture time on the mechanical properties (compressive modulus, equilibrium modulus, stress relaxation, dynamic modulus, and phase shift) of the cellular graphene composites was measured using a one-way MANOVA in SPSS ($p = 0.05$) using the Bonferroni correction for multiple comparisons.

Cellular Studies: GF (Graphene Laboratories Inc., Calverton, NY, USA) with a density of 4 mg cm^{-3} and an average pore size of 580 µm was cut into 1 × 1 cm pieces, sterilized in 70% ethanol, washed in sterile DPBS buffer, and incubated in growth medium (GM) composed of F12/Dulbecco's Modified Eagle Medium (DMEM), 5% (v/v) fetal bovine serum (FBS), and 100 U ml^{-1} penicillin, 100 µg ml^{-1} streptomycin (Life Technologies, Carlsbad, CA); in 5% CO_2 at 37 °C for 24 h before cell seeding. Conditioned GF was seeded with ATDC5 chondroprogenitor cells (Sigma-Aldrich, St. Louis, MO) and cultured for 24 h in growth media (F12/DMEM, 5% FBS) and incubated in 5% CO_2 at 37 °C. After 24 h, growth medium was exchanged with differentiation medium (DM) containing F12/DMEM, 5% FBS, 100 U ml^{-1} penicillin, 100 µg ml^{-1} streptomycin (Life Technologies, Carlsbad, CA), 50 µg ml^{-1} ascorbate-2-phosphate (Sigma-Aldrich, St. Louis, MO), and ITS supplement (0.01 mg mL^{-1} insulin, 5.5 ug mL^{-1} transferrin, and 5 ng mL^{-1} sodium selenite.; Sigma_Aldrich, St. Louis, MO). The DM was initially exchanged every two days until GF was confluent with cells at which time DM was exchanged daily. Throughout the ATDC5/GF cell culture, growth was monitored and representative images were collected using a Nikon TS-100 Microscope and SPOT R3 camera. Once samples were grown for 14 days and 28 days, they were subjected to mechanical testing to measure quasi-static and viscoelastic properties. One sample, following 28 days of growth was with 2% paraformaldehyde and transferred to a glass-bottom dish for immunostaining.

Immunofluorescence: ATDC5 cells grown on GF were permeabilized and blocked with 0.1% Triton X–100 (Sigma-Aldrich, St.Louis, MO) and BlockAid (Life Technologies, Carlsbad, CA), respectively. Cells were then labeled for cytoskeletal F-actin with Alexa Fluor 488 conjugated to phalloidin, mounted with ProLong Gold with DAPI to stain the nucleus (Life Technologies, Carlsbad, CA) and allowed to cure overnight before imaging.

Confocal Microscopy: Samples were imaged with the Zeiss LSM 510 Meta system combined with the Zeiss Axiovert Observer Z1 inverted microscope and ZEN 2009 imaging software (Carl Zeiss, Inc., Thornwood, NY). Confocal Z-stack and single plane images were acquired utilizing the Plan-Apochromat 20x/NA 0.8 and Fluar 40x/NA1.30 oil objectives; with a diode (405 nm) and an Argon (488 nm) laser sources. Transmitted light was also collected on a separate channel during the image acquisition to provide contrast to the GF structure. Image processing was performed with ZEN 2009 imaging software (Carl Zeiss, Inc., Thornwood, NY).

Supporting Information

Supporting Information is available from the Wiley Online Library or from the author.

Acknowledgements

Conflict of Interest

The authors declare no conflict of interest.

Keywords

[1] C. G. Helmick, D. T. Felson, R. C. Lawrence, S. Gabriel, R. Hirsch, C. K. Kwoh, M. H. Liang, H. M. Kremers, M. D. Mayes, P. A. Merkel, S. R. Pillemer, J. D. Reveille, J. H. Stone, *Arthritis Rheum*. **2008**, *58*, 15.

[2] M. Cross, E. Smith, D. Hoy, S. Nolte, I. Ackerman, M. Fransen, L. Bridgett, S. Williams, F. Guillemin, C. L. Hill, L. L. Laslett, G. Jones, F. Cicuttini, R. Osborne, T. Vos, R. Buchbinder, A. Woolf, L. March, *Ann. Rheum. Dis*. **2014**, *73*, 1323.

[3] R. Tuan, *Arthritis Res. Ther*. **2007**, *9*, 109.

[4] R. M. Schulz, A. Bader, *Eur. Biophys. J*. **2007**.

[5] D. D. Frisbie, J. T. Oxford, L. Southwood, G. W. Trotter, W. G. Rodkey, J. R. Steadman, J. L. Goodnight, C. W. McIlwraith, *Clin. Orthop. Relat. Res*. **2003**, *407*, 215.

[6] J. L. Escobar Ivirico, M. Bhattacharjee, E. Kuyinu, L. S. Nair, C. T. Laurencin, *Engineering* **2017**, *3*, 16.

[7] F. Zeifang, D. Oberle, C. Nierhoff, W. Richter, B. Moradi, H. Schmitt, *Am. J. Sports Med*. **2010**, *38*, 924.

[8] L. Gao, R. McBeath, C. S. Chen, *Stem Cells* **2010**, *28*, 564.

[9] J. Liao, Y. Qu, B. Chu, X. Zhang, Z. Qian, *Sci. Rep*. **2015**, *5*, 9879.

[10] Y. Yang, C. Han, B. Jiang, J. Iocozzia, C. He, D. Shi, T. Jiang, Z. Lin, *Mater. Sci. Eng. R Rep.* **2016**, *102*, 1.

[11] F. Alvi, M. K. Ram, P. A. Basnayaka, E. Stefanakos, Y. Goswami, A. Kumar, *Electrochim. Acta* **2011**, *56*, 9406.

[12] S. Kumar, S. Kaushik, R. Pratap, S. Raghavan, *ACS Appl. Mater. Interfaces* **2015**, *7*, 2189.

[13] G. S. Kulkarni, K. Reddy, Z. Zhong, X. Fan, *Nat. Commun.* **2014**, *5*, 4376.

[14] E. Krueger, A. N. Chang, D. Brown, J. Eixenberger, R. Brown, S. Rastegar, K. M. Yocham, K. D. Cantley, D. Estrada, *ACS Biomater. Sci. Eng.* **2016**, *2*, 1234.

[15] S. W. Crowder, D. Prasai, R. Rath, D. A. Balikov, H. Bae, K. I. Bolotin, H.-J. Sung, *Nanoscale* **2013**, *5*, 4171.

[16] T. R. Nayak, H. Andersen, V. S. Makam, C. Khaw, S. Bae, X. Xu, P. L. R. Ee, J. H. Ahn, B. H. Hong, G. Pastorin, B. Özyilmaz, *ACS Nano* **2011**, *5*, 4670.

[17] A. Nieto, R. Dua, C. Zhang, B. Boesl, S. Ramaswamy, A. Agarwal, *Adv. Funct. Mater.* **2015**, *25*, 3916.

[18] N. Li, Q. Zhang, S. Gao, Q. Song, R. Huang, L. Wang, L. Liu, J. Dai, M. Tang, G. Cheng, *Sci. Rep.* **2013**, *3*, 1604.

[19] M. E. Wechsler, B. P. Hermann, R. Bizios, *Tissue Eng. Part C Methods* **2015**, *22*, 155.

[20] V. C. Mow, X. E. Guo, *Annu. Rev. Biomed. Eng.* **2002**, *4*, 175.

[21] X. Yuan, D. E. Arkonac, P. G. Chao, G. Vunjak-Novakovic, *Sci. Rep.* **2014**, *4*, 3674.

[22] D. E. Discher, P. Janmey, Y.-L. Wang, *Science* **2005**, *310*, 1139.

[23] A. J. Engler, S. Sen, H. L. Sweeney, D. E. Discher, *Cell* **2006**, *126*, 677.

[24] W. Park, X. Li, N. Mandal, X. Ruan, Y. P. Chen, *APL Mater.* **2017**, *5*, 1.

[25] W. Xie, F. Song, R. Wang, S. Sun, M. Li, Z. Fan, B. Liu, Q. Zhang, J. Wang, *Crystals* **2018**, *8*, 105.

[26] Q. Yao, J. Jing, Q. Zeng, T. L. Lu, Y. Liu, X. Zheng, Q. Chen, *ACS Appl. Mater. Interfaces* **2017**, *9*, 39962.

[27] X. Dong, X. Wang, L. Wang, H. Song, H. Zhang, W. Huang, P. Chen, *ACS Appl. Mater. Interfaces* **2012**, *4*, 3129.

[28] B. Lu, T. Li, H. Zhao, X. Li, C. Gao, S. Zhang, E. Xie, *Nanoscale* **2012**, *4*, 2978.

[29] M. Shahnawaz Khan, H. N. Abdelhamid, H. F. Wu, *Colloids Surf. B Biointerfaces* **2015**, *127*, 281.

[30] A. Nieto, B. Boesl, A. Agarwal, *Carbon N. Y.* **2015**, *85*, 299.

[31] C. J. Little, N. K. Bawolin, X. Chen, *Tissue Eng. Part B Rev.* **2011**, *17*, 213.

[32] J. A. Panadero, V. Sencadas, S. C. M. Silva, C. Ribeiro, V. Correia, F. M. Gama, J. L. Gomez Ribelles, S. *Lanceros-Mendez, J. Biomed. Mater. Res. — Part B Appl. Biomater.* **2016**, *104*, 330.

[33] P. Nautiyal, B. Boesl, A. Agarwal, *Small* **2017**, *13*, 1.

[34] D. Lahiri, S. Das, W. Choi, A. Agarwal, *ACS Nano* **2012**, *6*, 3992.

[35] P. Nautiyal, B. Boesl, A. Agarwal, *Carbon N. Y.* **2018**, *132*, 59.

[36] Y. Z. He, H. Li, P. C. Si, Y. F. Li, H. Q. Yu, X. Q. Zhang, F. Ding, K. M. Liew, X. F. Liu, *Appl. Phys. Lett.* **2011**, *98*, 3101.

[37] G. A. Ateshian, V. C. Mow, in: *Basic Orthopaedic Biomechanics and Mechano-Biology* (Eds: V. C. Mow, R. Huiskes), Philadelphia, US **2005**, pp. 447.

[38] J. K. Wang, G. M. Xiong, M. Zhu, B. Özyilmaz, A. H. Castro Neto, N. S. Tan, C. Choong, *ACS Appl. Mater. Interfaces* **2015**, *7*, 8275.

[39] Z. Chen, W. Ren, L. Gao, B. Liu, S. Pei, H.-M. Cheng, *Nat. Mater.* **2011**, *10*, 424.

[40] W. C. Lee, C. H. Y. X. Lim, H. Shi, L. A. L. Tang, Y. Wang, C. T. Lim, K. P. Loh, *ACS Nano* **2011**, *5*, 7334.

[41] S. M. Lien, L. Y. Ko, T. J. Huang, *Acta Biomater.* **2009**, *5*, 670.

[42] Y. Yao, Y. Wang, *J. Cell. Biochem.* **2013**, *114*, 1223.

[43] D. J. Responte, R. M. Natoli, K. A Athanasiou, *Crit. Rev. Biomed. Eng.* **2007**, *35*, 363.

[44] Y. A. Samad, Y. Li, S. M. Alhassan, K. Liao, *ACS Appl. Mater. Interfaces* **2015**, *7*, 9196.

[45] C. Wang, D. Pan, S. Chen, *Carbon N. Y.* **2018**, *132*, 641.

[46] C. Wang, C. Zhang, S. Chen, *Carbon N. Y.* **2016**, *109*, 666.

[47] K. Saini, N. Kumar, *Mater. Sci. Eng. C* **2015**, *49*, 720.

[48] V. C. Mow, A. F. Mak, W. M. Lai, L. C. Rosenberg, L. H. Tang, *J. Biomech.* **1984**, *17*, 325.

[49] A. J. Nixon, E. Rickey, T. J. Butler, M. S. Scimeca, N. Moran, G. L. Matthews, *Osteoarthr. Cartil.* **2015**, *23*, 648.

[50] D. J. Griffin, E. D. Bonnevie, D. J. Lachowsky, J. C. A. Hart, H. D. Sparks, N. Moran, G. Matthews, A. J. Nixon, I. Cohen, L. J. Bonassar, *J. Biomech.* **2015**, *48*, 1944.

[51] L. Cao, F. Zhang, Q. Wang, X. Wu, *Mater. Sci. Eng. C* **2017**, *79*, 697.

[52] V. Singh, D. Joung, L. Zhai, S. Das, S. I. Khondaker, S. Seal, *Prog. Mater. Sci.* **2011**, *56*, 1178.

[53] T. J. Lujan, C. J. Underwood, N. T. Jacobs, J. A. Weiss, *J. Appl. Physiol.* **2008**, *106*, 423.